Spatial mapping of time-variable errors in Jason-1 and TOPEX/POSEIDON sea surface height measurements

Rui M. Ponte
Atmospheric and Environmental Research, Inc., Lexington, Massachusetts, USA

Carl Wunsch
Massachusetts Institute of Technology, Cambridge, USA

Detlef Stammer
Zentrum für Meeres- und Klimaforschung, Universität Hamburg, Germany

18/July/2006

Abstract. Fitting ocean models to altimeter sea surface height (SSH) measurements requires knowledge of instrument noise (radar noise, sea state bias, path delay corrections, and orbit errors) and "representation" errors related to SSH signals (e.g., tidal or pressure-driven) not computed in the models. Comparisons between the independent TOPEX/POSEIDON and Jason-1 altimetric missions when they were in identical orbits show that point-by-point the data are consistent within the mission specifications of about 3 cm rms, but large-scale dependences exist in the data differences, and these are both poorly known and capable of introducing major errors into oceanic state estimates. Here we focus on the time-variable component of the spatially dependent errors. The analysis reveals errors ranging from 2 cm in the tropics to 4 cm at mid and high latitudes and roughly consistent with a dependence of instrument noise on significant wave height. Analysis of the representation errors suggests that, over the deep ocean, uncertainties associated with the simplifying assumption of an inverted barometer response to pressure loading are larger than the remaining errors in modeling the large-scale tides. Over extensive regions, however, errors associated with eddy signals missing in coarse resolution models can dominate. Obtaining a more quantitative estimate of the latter errors remains a challenge.

1. Introduction

Satellite altimetry has become an essential tool in oceanography as it provides the only existing near-global, time-continuous measurements. As with all observational systems, an estimate of the errors in altimeter sea surface height (SSH) observations is essential for quantitative use of the data. In general, the data are analyzed directly (e.g., as in frequency-wavenumber spectral estimates), or used to constrain general circulation models in a least-squares sense. In most applications, the data are separated into a time-mean sea surface (MSS) and anomalies about that mean. When the MSS is combined with a geoid height surface, one has an estimate of the absolute, time average surface dynamic topography [e.g., *Wunsch and Stammer*, 1998]. Temporal anomalies about the surface dynamic topography are independent of the geoid, which has its own error budget, but nonetheless contain various complex corrupting elements.

The immediate motivation for this note is the need to define altimeter errors in a global ocean state estimation system (called Estimating the Circulation and Climate of the Ocean—ECCO [see *Stammer et al.*, 2002; *Köhl et al.,* 2006; *Wunsch and Heimbach, 2006*]; the particular calculations will be referred to as the MIT-AER estimates because the ECCO effort has several independent strands). A general circulation model is fit explicitly in a weighted least-squares sense to the altimetric measurements from several different satellites. As in any least-squares problem, the solution can be no better than the accuracy with which data (and model) errors are represented. If underestimating errors, one fits noise; if over-estimating them, one is discarding useful information. The same error field estimates are useful in any more direct use of the data, and elements of the error estimates simultaneously provide useful descriptions of the ocean (its time-dependent variances, wave heights, etc.).

Although the on-going ECCO calculations use data from the TOPEX/POSEIDON, Jason-1, ERS-1,2 and Envisat missions, we focus here on understanding of the TOPEX/POSEIDON (hereafter TP) and Jason-1 data, as these provide the basic

calibration for all the other altimeters [*Le Traon et al.*, 2003] and have been the subject of the most intense scrutiny. Knowledge of the error budget for TP is summarized in *Chelton et al.* [2001; hereafter denoted C2001]. Their Table 11 contains estimates for various error sources: altimeter radar noise; electromagnetic and skewness biases, which together make up the so-called sea state bias (SSB); ionospheric, wet and dry tropospheric corrections—all are part of the environmental effects that cause signal path delays; and orbit error. C2001 specified the total (mean and time-variable) error for each of these terms separately, with the largest being orbit error (2.5 cm), and the combined root-sum-square (rss) error was estimated at 4.1 cm. (Numbers in C2001 refer specifically to the dual-frequency TOPEX altimeter; the single-frequency POSEIDON altimeter is slightly more noisy and has a more uncertain ionospheric correction [*Fu et al.,* 1994] but such a distinction will be ignored here.) Although only globally averaged values are given, their comprehensive discussion of each error source indicates that several of them are expected to have considerable spatial dependence [see also *Tsaoussi and Koblinsky*, 1994]—a dependence which is the main focus here as it is of prime importance in global estimation problems.

The launch of Jason-1 in 2001 and the "tandem mission" with TP, during which the altimeters were flying about 70s apart in identical orbits and thus sampling essentially the same ocean variability, provided an unusual opportunity for altimeter comparison and cross-calibration. These efforts are discussed in six dedicated numbers of Marine Geodesy (Vol. 26, 3–4; Vol. 27, 1–4). *Ménard et al.* [2003] show globally-averaged errors for Jason-1 similar to those of TP [C2001], apart from a somewhat lower orbit error (1.5 cm), and a total rss error of 3.3 cm, well within the pre-launch specifications for Jason-1. In that sense, the engineering specifications for the missions have been more than met. Sufficiently small pointwise error differences are, however, a necessary, but not sufficient, prescription of errors. If large-scale (geographically correlated) errors exist, even though bounded at any given point, they can give rise to serious estimation

errors in any analysis, or least-squares fit to the observations.

Geographically-dependent errors in altimetry have been discussed primarily in the context of time mean (systematic, or bias) differences between TP and Jason-1 [*Beckley et al.*, 2004; *Dorandeu et al.*, 2004; *Chambers et al.*, 2004], with orbit and SSB errors found to be partly to blame. *Han* [2004] analyzes root-mean-square (rms) differences, but only for a small region off Nova Scotia. Regional error budgets, focusing on time-variable terms, have not been much considered. Exceptions are the studies of *Le Traon and Dibarboure* [2004] and *Whitmer et al.* [2004], but the former is based on data that is substantially smoothed in time and space while the latter is based on crossover analyses that assume high frequency signals to be part of the error.

In this note, a more direct and simpler approach is used to infer geographical dependence of altimeter noise. Spatial correlations are not explicitly dealt with; we seek to map regions of error significantly larger or smaller than the space-time average. Finding estimates of actual space/time correlations within and between such regions is a far more demanding task than the one described here. The focus is on errors affecting the time-variable SSH, with systematic biases (including geoid problems) treated elsewhere [*Stammer et al.*, 2005 specifically discuss the geoid error]. As will be seen, the story remains incomplete, and this work is in part an attempt to stress the need for more complete modeling of altimeter data uncertainties.

2. Time-variable instrument noise

We consider SSH errors intrinsic to the altimeter measurement (i.e., range noise), involving radar noise, SSB errors, uncertainties in ionospheric, wet and dry tropospheric corrections, and orbit error. Our analysis is based on point measurements at 1Hz sampling rate, which is the basic altimeter data set. Smoothed products are discussed at the end.

Here we use two different methods to arrive at an approximate determination

of spatial dependences in the range measurement errors. In one approach, we take advantage of the TP and Jason-1 tandem mission. The particular TP and Jason-1 SSH data sets used here are described in the Appendix. Differences between the two inferred SSH estimates can be interpreted as representing differences between instrument errors in the two altimeters. This method provides an easy way of separating time mean and variable errors, which is convenient, given our need to estimate errors on SSH anomalies. Some assumptions about the partition of errors between instruments are required. Along-track and crossover analyses suggest slightly noisier Jason measurements compared to TP, mostly related to differences at wavelengths shorter than 50 km [*Dorandeu et al.*, 2004]. For simplicity, we ignore any small differences in Jason and TP instrument performance and assume an approximate equipartition of error variance.

The standard deviation of the differences, TP minus Jason, based on 1Hz range estimates, is shown in Fig. 1a. A description of the temporal and spatial characteristics of the variability in the difference series is beyond our scope, but we note that empirical orthogonal function analysis of 10-day TP−Jason maps (not shown) suggests a wide range of space and time scales, including very long (basin scale) patterns indicative of spatially correlated errors. The standard deviation in Fig. 1a is interpreted as representing the combined effects of orbit errors and radar noise, and also errors in SSB, ionospheric and wet tropospheric corrections, which are instrument-dependent. Estimates in Fig. 1a are somewhat noisy at the shortest scales, which probably reflects the relatively small amount of data (only 20 orbit repeat cycles or ∼200 days) available for the TP−Jason series. Notice also that the relatively short record duration may affect the separation of time-variable errors from those in the mean, as the stability of the mean is a function of the averaging time.

Errors in the dry tropospheric correction are not included in Fig. 1a, as the same atmospheric pressure field is used in correcting both altimeters. A separate estimate of the uncertainty in the dry tropospheric correction is shown in Fig. 1b. Values

correspond to 23% of the errors in the pressure field [C2001], which are estimated based on the standard deviation of the difference between ECMWF and NCEP operational analysis for the years 2001-2003, and assuming equipartition of errors between the analyses [*Salstein et al.*, 2006]. The difference between analyses likely defines a lower bound on the uncertainty of the pressure fields, because possible common errors are removed by subtraction. Errors in the dry tropospheric correction are < 0.5 cm, except in high southern latitudes, and thus small compared to other errors (cf. Fig. 1a). *Fu et al.* [1994] estimate it as a constant, 0.7 cm, based on a value of 3 cm rms error in the pressure fields. Estimates in Fig. 1b are lower, and indicate improvements in the weather center analyses over the last few years; for the early years of TP, these errors are likely larger than the estimates in Fig. 1b [*Ponte and Dorandeu*, 2003; *Salstein et al.*, 2006]).

The total error, given in Fig. 1c, mostly resembles the pattern in Fig. 1a, divided by $\sqrt{2}$ to account for uncertainty in one altimeter only. There is a clear increase in errors as one moves poleward, with a typical range from $\sim$2 cm in the tropics to $\sim$4 cm at high latitudes, and comparable to the average error of 4.1 cm quoted by C2001. The latter represents the total error and is expected to be larger than the time-dependent component alone. However, estimates of the rms difference of TP and Jason are not that different from those in Fig. 1a, i.e., TP/Jason comparisons suggest that the total error is dominated by its time variable component.

The spatial pattern in Fig. 1c is consistent with the expected dependence of noise levels on significant wave height (S_w), which tends to be largest at middle and high latitudes [C2001]. An independent method of estimating the errors consists of modeling radar and SSB noise using known relationships with S_w. Based on Fig. 2 of *Vincent et al.* [2003], radar noise r_n is linearly related to S_w as

$$r_n = a + bS_w$$

with S_w given in meters and a ~1.21 cm, b ~0.18 cm/m. Values are appropriate for 1Hz measurements. The standard deviation of the time-dependent noise is then $b\sigma_{S_w}$, where σ_{S_w} denotes the standard deviation of S_w in meters. Errors in the SSB correction are similarly related to S_w. C2001 suggest an uncertainty in SSB correction of approximately 1% of S_w. These relations are expected to apply to both TP and Jason [*Vincent et al.*, 2003].

Assuming radar and SSB noise are uncorrelated, their combined effect amounts to $\sim 1.02\sigma_{S_w}$. Values of σ_{S_w} have been calculated by C2001 from the first seven years of TP data (cf. their Fig. 36). To this estimate, one can add uncertainties in the dry tropospheric correction from Fig. 1b. There are no readily available spatial-dependence estimates for the remaining terms (wet tropospheric and ionospheric corrections, orbit error), and we use the values 1.1 cm, 0.5 cm, and 2.5 cm, respectively, from Table 11 of C2001, assuming they mostly represent time variable errors. (In principle, the ionospheric correction is also related to S_w [*Fu et al.,* 1994], but it is the smallest term in the error budget and a constant is sufficient for the current purposes.)

Combining all these effects leads to the rss error shown in Fig. 1d, which exhibits large-scale spatial patterns very similar to those in Fig. 1c. These patterns are largely explained by the dependence of radar and SSB noise on S_w [C2001]. The amplitudes in Figs. 1c,d are also quite consistent, although there is a tendency for larger errors in Fig. 1d at most latitudes. Note that contributions from the wet tropospheric and ionospheric correction errors, as well as orbit errors, may have been overestimated in Fig. 1d, given that numbers in C2001 represent total errors. Any spatial variability in these terms, not accounted for here, may also contribute to the differences with Fig. 1c. There is also an indication that because of recent improvements in precision orbit determination, current orbit errors are somewhat smaller than those quoted in C2001 [*Ménard et al.*, 2003]. In any case, the resulting error estimates from the two different methods are in reasonable agreement.

3. Representation errors in state estimation

This section will be of interest both to those engaged in state estimation using altimetric data with general circulation models, and also for anyone attempting to use altimetric data in isolation—models are necessarily used in any data analysis even if not explicitly noticed (e.g., an assumption that data are dominated by mesoscale eddies, rather than internal tides, is a model). Because model developers do not provide explicit forms for the errors incurred in their numerics, it is usually more convenient to rewrite model errors as data errors (e.g., any physical phenomenon appearing in the data but not in the model is a "representation" error). A quantitative description of representation errors is very difficult, as it involves knowledge of data statistics and model characteristics and is specific to each particular problem. In the MIT-AER ECCO $1^\circ \times 1^\circ$ model forced by wind stress and heat and freshwater fluxes [e.g., *Wunsch and Heimbach*, 2006], we attempt to account for three major representation errors of altimetric data, namely those related to ocean tides and atmospheric pressure-driven signals, which are of general interest to all altimeter data users, and unresolved eddy variability.

Tides

Altimeter data are routinely corrected for tides and thus errors from this term are present insofar as the tide models are not perfect. A typical value for deep ocean tide model errors is 2 cm rms with part of it likely related to omission of internal tides [*Shum et al.*, 1997]. The latter will diminish strongly in the $1^\circ \times 1^\circ$ averages. Large scale errors cannot be excluded, however. For example, orbit errors are known to include tidal components, some minor tides are omitted, etc. Absent adequate information, we use a constant value of 1 cm for the representation error in deep-sea tides. (Tide errors over shallow water are certainly much higher. A crude spatially variable estimate can be obtained from differencing the two tide models available with the altimeter data sets, but the results are not displayed here.)

Atmospheric Pressure Load

Altimeter data are similarly corrected for pressure-driven signals using a simple inverted barometer (IB) correction (~1 cm/hPa; C2001). Errors in pressure fields and omission of any dynamic signals both contribute here. For the IB error, as for the dry tropospheric correction, we base again our lower-bound estimate on the standard deviation of differences between ECMWF and NCEP pressure fields. Thus, IB errors are approximately four times larger than the values for the dry tropospheric correction, shown in Fig. 1b.

An estimate of dynamic signals resulting from atmospheric loading can be obtained from the modeling experiments of *Ponte and Vinogradov* [2006]. A one-year run of a simplified version of the ECCO general circulation model forced by pressure forcing alone gives the standard deviation values in Fig. 2a, which are similar to previous estimates from purely barotropic models [*Ponte*, 1993]. Results in Fig. 2a do not include effects of the mean (climatological) S_1 and S_2 air tide forcing, which were removed from the forcing fields [*Ponte and Vinogradov*, 2006]. These effects should be accounted for as part of the tide model correction, but currently S_1 is not included in those corrections (to be added in future data releases). An amplitude estimate for the latter tide [*Ponte and Vinogradov*, 2006] is shown in Fig. 2b. Results are very similar to those of *Ray and Egbert* [2004]. The combined error from pressure-forced dynamic signals, based on Fig. 2a,b, is shown in Fig. 2c. Apart from shallow regions, typical values are 2-3 cm, which are larger than our assumed tide errors.

Mesoscale Eddies

The remaining term in the time-dependent error is a consequence of unresolved eddy variability in the model and as already noted, can be regarded as either a data or a model error. As will be seen it is likely the dominant time-dependent error for present purposes, but unfortunately it is difficult to estimate, in part because there is no clear operational definition of "eddy". For simplicity, the following procedure was used. First,

the "signal" variance in the altimeter data was estimated by subtracting the computed error variance (instrument noise from Fig. 1d plus representation errors related to tides and atmospheric pressure load as discussed above) from the observed TP and Jason-1 altimeter variance based on 1Hz measurements. A percentage of such "signal" variance is associated with unresolved eddies. An estimate of that percentage was obtained by comparing the variance from an eddy-resolving (1/8°) version of the ECCO model [D. Menememlis, private communication, 2005] to that from the 1° MIT-AER ECCO runs. The percentage of eddy variance was calculated as $100 \times (\sigma^2_{1/8^\circ} - \sigma^2_{1^\circ})/\sigma^2_{1/8^\circ}$, where the σ^2_j refer to the variances of the two models. (The two models differ in a number of ways apart from their grid resolutions —in particular, the eddy-resolving runs are not constrained to any ocean data— but the assumption that the difference in variance is mostly due to eddy effects seems a reasonable one.)

The resulting estimate for the eddy error term (Fig. 2d) can reach values > 30 cm in western boudary regions with vigorous current systems and is also enhanced along the path of the Antarctic Circumpolar Current. Values in quiet interior regions (tropics, eastern basins) are mostly < 5 cm, but not zero. The total representation error (tides+pressure signals+eddies; not shown) is dominated by the eddy term as expected and resembles closely Fig. 2d. For eddy-resolving modeling efforts, the situation would be somewhat different, with other representation errors becoming more important.

4. Summary remarks

The combination of instrument noise and representation errors yields the estimate of total error shown in Fig. 3. Here, we have taken the instrument noise based on S_w (Fig. 1d), but results are similar when using estimates based on the TP−Jason analysis (Fig. 1c). In addition, the correlation between errors in dry tropospheric correction and IB effect has been neglected. Representation errors dominate the total budget and thus the spatial pattern in Fig. 3 follows closely that of Fig. 2d. Instrument errors contribute

to raise the noise levels mainly in interior regions where our estimate of eddy errors is comparable to that of instrument noise. Estimates in Fig. 3 are probably relatively robust in boundary current regions, whereas levels in the interior may be too high. The underlying issue is whether eddies can be as important everywhere as the 1/8° to 1° model comparison seems to suggest.

Lower error values will result when considering data averaged along track over 1° boxes, as is used in the MIT-AER ECCO estimation procedure, instead of 1Hz measurements. One can calibrate the errors in Fig. 3 by comparing the standard deviation of TP or Jason-1 data based on 1Hz data with that based on along-track averaged data. For averaging over 2° boxes (1° could be tried but there would be many boxes without data), typical reduction in TP standard deviation is 10% to 20%, which can be assumed for simplicity to result from proportional decreases in signal and noise variance. For the estimated error adjusted for the effects of data smoothing, one can reduce the values in Fig. 3 by equivalent amounts.

A more involved step-by-step calibration could also be used. For instrument noise, changes would involve calculating TP−Jason difference based on along-track averages or reducing components that are likely to be attenuated by the averaging (radar noise, SSB, possibly wet tropospheric correction, ionospheric correction errors already estimated based on ∼100 km arcs). For representation errors, one could use altimeter standard deviations based on averaged along-track data for the calculation of eddy term.

The results in Fig. 3 are the basis for the errors currently used in the MIT-AER ECCO estimates to control the model/altimeter data misfits. As it is dominated by the eddy error term, the same figure represents an estimate of the mesoscale eddy variability in the ocean, which is currently not resolved in the ECCO model. The present results are not, and cannot be, definitive as they are dependent upon elements of the altimetric system noise which are poorly known. They are presented here at this time as being our best global estimates (which we use), in the hope that they may be helpful to others

and that they may stimulate further work on this important data set.

Acknowledgments. We thank L.-L. Fu (JPL) for suggestions on how to address the spatial structure of altimeter errors, D. Chelton (OSU) for the significant wave height data, K. Case (JPL) for clarifications on the altimeter dataset, D. Menemenlis (JPL) for the output of the 1/8° model, and C. King (MIT) for help with data processing. Supported by NASA through the Jet Propulsion Laboratory Jason-1 program, and by the National Ocean Partnership Program (NOPP) of NASA, NSF, and NOAA.

Appendix: Altimeter data

The SSH altimeter series used are the TP and Jason-1 Along-Track-Gridded Sea Surface Height Anomaly products provided by the Physical Oceanography DAAC at the Jet Propulsion Laboratory. Both series are generated from the Geophysical Data Record (GDR), using the respective GDR orbits, and given at 1Hz sampling. TP and Jason-1 anomalies are defined relative to the same MSS and both series are corrected for tides using the same model (GOT99.2b). All geophysical corrections available on the GDR have been applied, with the exception of the SSB correction for the case of TP, which is replaced as recommended in *Chambers et al.* [2003]. In addition, the ionospheric correction used is based on values smoothed over approximately 100 km along track, centered on the location of the data value. The smoothing reduces the uncertainty in the ionospheric correction and is consistent with commonly quoted errors for that correction [*Chelton et al.,* 2001]. Further information on the data processing of the TP and Jason-1 Along-Track-Gridded Sea Surface Height Anomaly products can be found in the documentation available at the original archival site.

During the first 20 cycles of Jason-1, both altimeters flew along the same ground track separated in time by ~70 s. Data from this period was used to construct the difference series used in Fig. 1a. Given the described data processing, corrections for tides, the inverted barometer effect and path delay by the dry troposphere are essentially the same in TP and Jason-1 series, as they are based on the same tide and atmospheric pressure models. The differences in the TP and Jason-1 anomaly series at the same along-track points are thus taken to represent mostly radar noise, other instrument errors related to the ionospheric, wet tropospheric, and SSB corrections, and orbit error. The results in Fig. 1a represent the averaged instrument noise without considering possible differences between ascending and descending tracks, which are known to affect the calculation of the bias between TP and Jason-1 (e.g., see posters by Philipps et al. and others presented at the March 2006 Ocean Surface Topography Science Team Meeting in Venice; available at http://www.jason.oceanobs.com/documents/swt/posters2006/).

A number of reprocessed TP and Jason-1 data sets became available in early 2006, after

our original data analysis was performed. Judging from preliminary comparisons discussed at the Venice meeting, the reprocessed data should lead to reduced TP and Jason differences, but large changes from the standard deviation values in Fig. 1a are not expected (e.g., see again the poster by Phillips et al.). In any case, estimates of the altimeter noise provided here will necessarily have to be updated as improved data sets continue to be produced.

References

Beckley, B.D., N.P. Zelensky, S.B. Luthcke, and P.S. Callahan, 2004: Towards a seamless transition from TOPEX/Poseidon to Jason-1, *Mar. Geod.*, **27**, 373–389.

Chambers, D.P., S.A. Hayes, J.C. Ries, and T.J. Urban, 2003: New TOPEX sea state bias models and their effect on global mean sea level. *J. Geophys Res.*, **108**, 3305,doi:10.1029/2003JC001839.

Chambers, D. P., J. C. Ries, and T. J. Urban, 2003: Calibration and verification of Jason-1 using global along-track residuals with TOPEX. *Mar. Geod.*, **26**, 305–317.

Chelton, D. B., J. C. Ries, B. J. Haines, L.-L. Fu, and P. S. Callahan, 2001: Satellite altimetry. In *Satellite Altimetry and Earth Sciences,* edited by L.-L. Fu and A. Cazenave, pp. 1–131, Academic Press, San Diego, Cal.

Dorandeu, J., M. Ablain, Y. Faugere, F. Mertz, B. Soussi, and P. Vincent, 2004: Jason-1 global statistical evaluation and performance assessment: calibration and cross-calibration results. *Mar. Geod.*, **27**, 345–372.

Fu, L.-L., E.J. Christensen, C.A. Yamarone Jr., M. Lefebvre, Y. Ménard, M. Dorrer, and P. Escudier, 1994: TOPEX/POSEIDON mission overview. *J. Geophys. Res.*, **99**, 24,369–24,381.

Fu, L.-L. (ed.), 2004: Minutes of the Ocean Surface Topography Science Team meeting, November 4–6, 2004. Jet Propulsion Laboratory, Pasadena (JPL D-31211), pp. 78.

Han, G., 2004: TOPEX/Poseidon-Jason comparison and combination off Nova Scotia. *Mar. Geod.*, **27**, 577–595.

Köhl, A., D. Stammer, and B. Cornuelle, 2006: Interannual to decadal changes in the ECCO global synthesis. *J. Phys. Oceanogr.*, in press.

Le Traon, P.Y., and G. Dibarboure, 2004: An illustration of the contribution of the TOPEX/Poseidon-Jason-1 tandem mission to mesoscale variability studies. *Mar. Geod.*, **27**, 3–13.

Le Traon, P. Y., Y. Faugere, F. Hernandez, J. Dorandeu, F. Mertz, and M. Ablain, 2003: Can we merge Geosat follow-on with TOPEX/Poseidon and ERS-2 for an improved description of the ocean circulation? *J. Atmos. Oce. Tech.*, **20**, 889–895.

Ménard, Y., L.-L. Fu, P. Escudier, F. Parisot, J. Perbos, P. Vincent, S. Desai, B. Haines, and G. Kunstmann, 2003: The Jason-1 mission. *Mar. Geod.*, **26**, 131–146.

Ponte, R.M., 1993: Variability in a homogeneous global ocean forced by barometric pressure. *Dyn. Atmos. Oceans*, **18**, 209–234.

Ponte, R.M., and J. Dorandeu, 2003: Uncertainties in ECMWF surface pressure fields over the ocean in relation to sea level analysis and modeling. *J. Atmos. Oce. Tech.*, **20**, 301–307.

Ponte, R.M., and S.V. Vinogradov, 2006: Effects of stratification on the large-scale ocean response to barometric pressure. *J. Phys. Oceanogr.*, in press.

Ray, R.D., and G.D. Egbert, 2004: The global S_1 tide. *J. Phys. Oceanogr.*, **34**, 1922–1935.

Salstein, D.A., R.M. Ponte, and K. Cady-Pereira, 2006: Uncertainties in atmospheric surface pressure fields from global analyses. Submitted.

Shum, C.-K., and co-authors, 1997: Accuracy assessment of recent ocean tide models. *J. Geophys. Res.*, **102**, 25173–15194.

Stammer, D., A. Köhl, and C. Wunsch, 2005: Tests of geoid height skill through estimates of the ocean circulation. To be published.

Stammer, D., C. Wunsch, R. Giering, C. Eckert, P. Heimbach, J. Marotzke, A. Adcroft, C.N. Hill and J. Marshall, 2002: The global ocean circulation during 1992–1997, estimated from ocean observations and a general circulation model. *J. Geophys. Res.*, **107**, 3118, doi:10.1029/2001JC000888.

Tsaoussi, L.S., and C.J. Koblinsky, 1994: An error covariance model for sea surface topography and velocity derived from TOPEX/POSEIDON altimetry. *J. Geophys. Res.*, **99**, 24669–24683.

Vincent, P., S.D. Desai, J. Dorandeu, M. Ablain, B. Soussi, P.S. Callahan, and B.J. Haines, 2003: Jason-1 geophysical performance evaluations. *Mar. Geod.*, **26**, 167–186.

Whitmer, K.R., G. A. Jacobs, and O.M. Smedstad, 2004: Altimeter signal-to-noise for deep ocean processes in operational systems, *Mar. Geod.*, **27**, 433–451.

Wunsch, C., and P. Heimbach, 2006: Practical global oceanic state estimation. Physica D, in press.

Wunsch, C., and D. Stammer, 1998: Satellite altimetry, the marine geoid, and the oceanic general circulation. *Annu. Rev. Earth Planet. Sci.*, **26**, 219–253.

R. M. Ponte, Atmospheric and Environmental Research, Inc., 131 Hartwell Avenue, Lexington, MA 02421-3126 USA. (e-mail: ponte@aer.com)

C. Wunsch, Massachusetts Institute of Technology, 77 Massachusetts Avenue, Cambridge, MA 02139 USA. (e-mail: cwunsch@ocean.mit.edu)

D. Stammer, Institut für Meereskunde, Universität Hamburg, Bundesstr. 53 20146 Hamburg, Germany. (e-mail: stammer@ifm.uni-hamburg.de)

Figure 1. Standard deviation (cm) of: (a) the TP minus Jason-1 series, computed for 20 cycles of the tandem mission and then averaged in $2^\circ \times 2^\circ$ boxes; (b) the error associated with the dry tropospheric correction; (c) the total instrument noise calculated as the rss of values in (a) divided by $\sqrt{2}$ and (b); (d) the altimeter noise computed from S_w as explained in the text. This paper is focused on understanding these large-scale patterns of errors, but not their space-time correlation structure.

Figure 2. (a) Standard deviation of dynamic signals forced by surface atmospheric pressure; (b) amplitude of the S_1 tide forced by the respective climatological air tide; (c) standard deviation of the error associated with variability in (a) and (b); (d) standard deviation of "eddy" error. All values given in cm.

Figure 3. Standard deviation (cm) of summed errors discussed in the text, and our best current estimate of the spatial structure of the altimetric errors. This pattern, reduced by 10% to account for data smoothing effects discussed in the text, is now used in the MIT-AER ECCO runs and corresponds to the diagonal of the error covariance matrix for the time-dependent altimetry. Off-diagonal elements have not yet been estimated. The figure can also be interpreted as an estimate of mesoscale variability in the ocean.

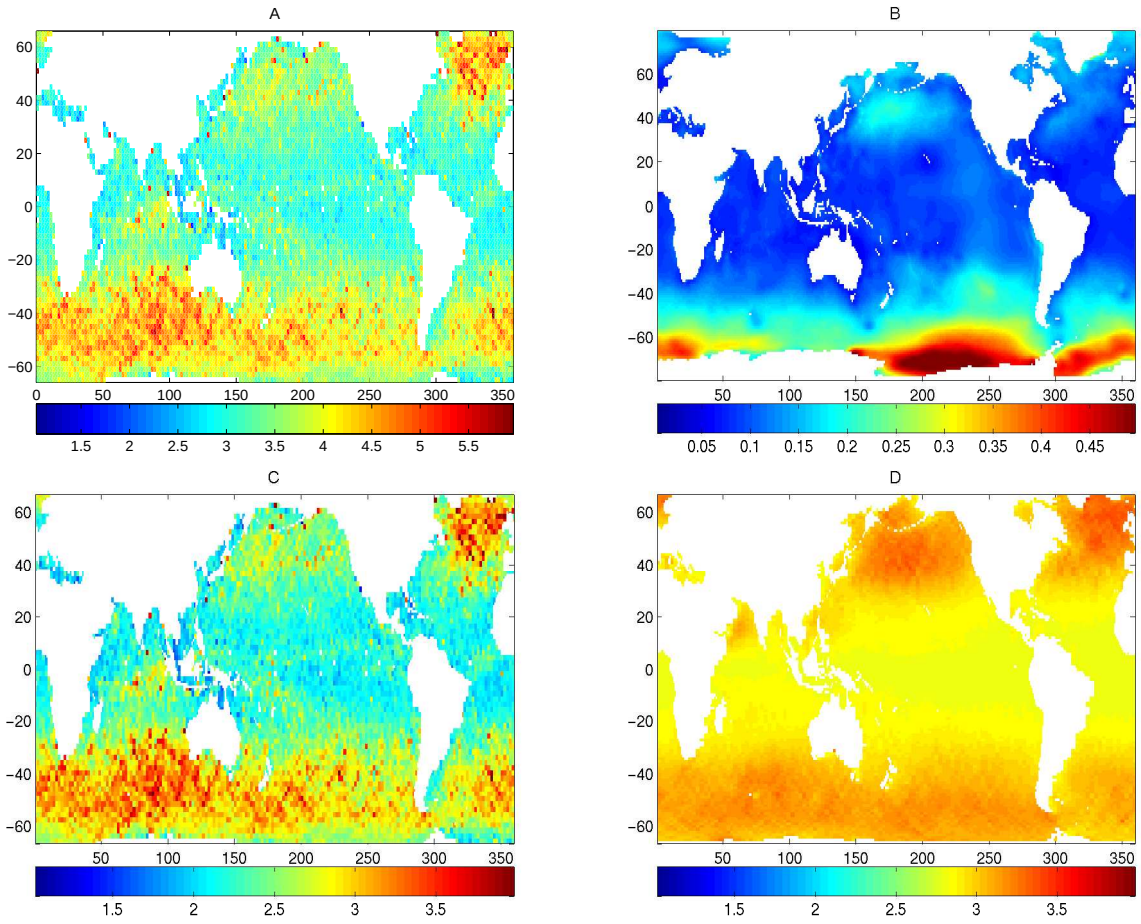

Figure 1. Standard deviation (cm) of: (a) the TP minus Jason-1 series, computed for 20 cycles of the tandem mission and then averaged in $2^\circ \times 2^\circ$ boxes; (b) the error associated with the dry tropospheric correction; (c) the total instrument noise calculated as the rss of values in (a) divided by $\sqrt{2}$ and (b); (d) the altimeter noise computed from S_w as explained in the text. This paper is focused on understanding these large-scale patterns of errors, but not their space-time correlation structure.

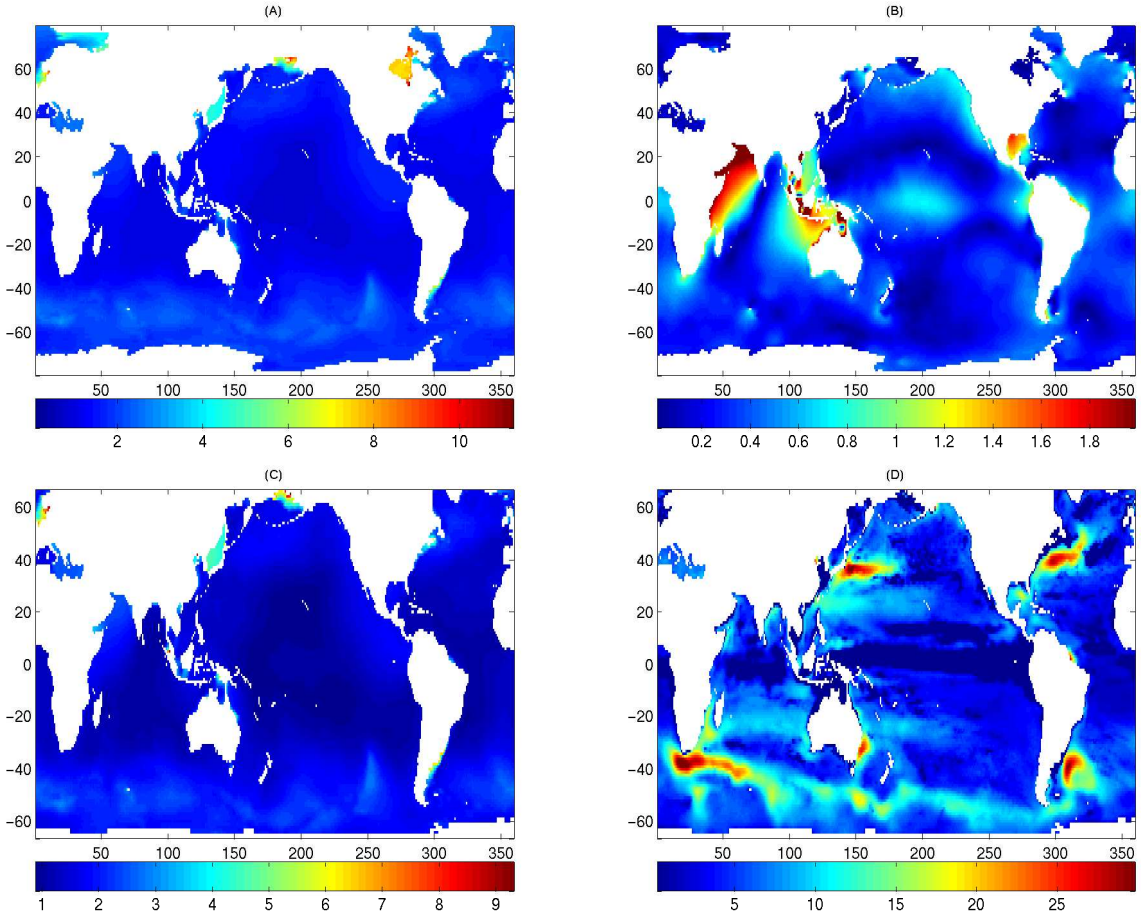

Figure 2. (a) Standard deviation of dynamic signals forced by surface atmospheric pressure; (b) amplitude of the S_1 tide forced by the respective climatological air tide; (c) standard deviation of the error associated with variability in (a) and (b); (d) standard deviation of "eddy" error. All values given in cm.

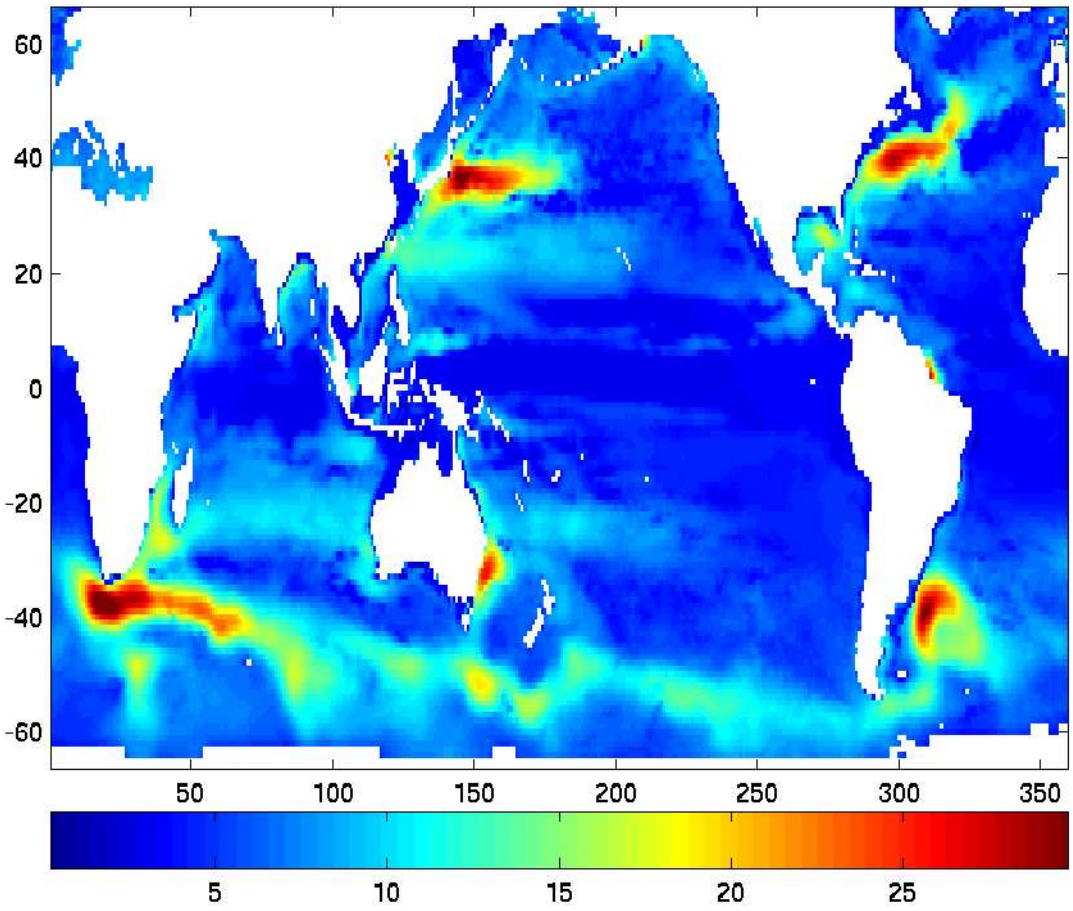

Figure 3. Standard deviation (cm) of summed errors discussed in the text, and our best current estimate of the spatial structure of the altimetric errors. This pattern, reduced by 10% to account for data smoothing effects discussed in the text, is now used in the MIT-AER ECCO runs and corresponds to the diagonal of the error covariance matrix for the time-dependent altimetry. Off-diagonal elements have not yet been estimated. The figure can also be interpreted as an estimate of mesoscale variability in the ocean.